



THE UNIVERSITY *of* EDINBURGH

Edinburgh Research Explorer

Ultrastable shelled PFC nanobubbles

Citation for published version:

Hanieh, PN, Ricci, C, Bettucci, A, Marotta, R, Moran, CM, Cantù, L, Carafa, M, Rinaldi, F, Del Favero, E & Marianecci, C 2022, 'Ultrastable shelled PFC nanobubbles: a platform for ultrasound-assisted diagnostics and therapy', *Nanomedicine: Nanotechnology, Biology and Medicine*.
<https://doi.org/10.1016/j.nano.2022.102611>

Digital Object Identifier (DOI):

[10.1016/j.nano.2022.102611](https://doi.org/10.1016/j.nano.2022.102611)

Link:

[Link to publication record in Edinburgh Research Explorer](#)

Document Version:

Peer reviewed version

Published In:

Nanomedicine: Nanotechnology, Biology and Medicine

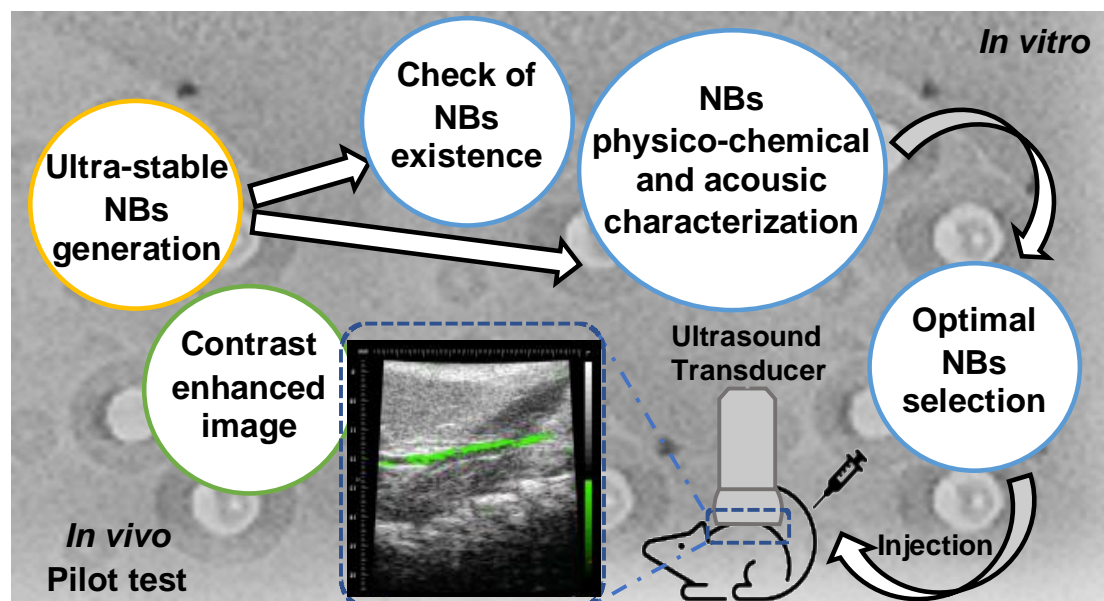
General rights

Copyright for the publications made accessible via the Edinburgh Research Explorer is retained by the author(s) and / or other copyright owners and it is a condition of accessing these publications that users recognise and abide by the legal requirements associated with these rights.

Take down policy

The University of Edinburgh has made every reasonable effort to ensure that Edinburgh Research Explorer content complies with UK legislation. If you believe that the public display of this file breaches copyright please contact openaccess@ed.ac.uk providing details, and we will remove access to the work immediately and investigate your claim.





Graphical abstract:

Ultra-stable NBs generation has been achieved by the optimization of a novel preparation method. These systems have been deeply characterized to assess NBs existence, in terms of physical chemical and acoustic features. The selected NBs had been tested in both *in vitro* and *in vivo* experiments, checking their capability as a potential platform for the production of versatile carriers to be used in ultrasound-assisted diagnostic, therapeutic, and theranostic applications.

Graphical Abstract:
Image

Ultra-stable
NBs
generation

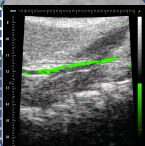
Check of
NBs
existence

Click here to
access/download; Gra

physico-chemical
and acousic
characterization

In vitro

Contrast
enhanced
image



Ultrasound
Transducer

Optimal
NBs
selection

In vivo
Pilot test



Injection

[Click here to view linked References](#)

Ultrastable shelled PFC nanobubbles: a platform for ultrasound-assisted diagnostics, and therapy

Patrizia Nadia Hanieh¹‡, Caterina Ricci²‡, Andrea Bettucci³, Roberto Marotta⁴, Carmel Mary Moran⁵, Laura Cantù², Maria Carafa¹, Federica Rinaldi^{1*}, Elena Del Favero^{2*}, Carlotta Marianecci¹

¹ Department of Drug Chemistry and Technology, Sapienza University of Rome, Piazzale A. Moro 5, 00185, Rome, Italy, patrizianadia.hanieh@uniroma1.it, federica.rinaldi@uniroma1.it, carlotta.marianecci@uniroma1.it, maria.carafa@uniroma1.it.

² Department of Medical Biotechnologies and Translational Medicine, University of Milan, Via Fratelli Cervi 93, 20090, Segrate, Italy, caterina.ricci@unimi.it, laura.cantu@unimi.it, elena.delfavero@unimi.it

³ Department of Basic and Applied Sciences for Engineering, Sapienza University of Rome, Via A. Scarpa 16, 00185, Rome, Italy, andrea.bettucci@uniroma1.it.

⁴ Italian Institute of Technology, Via Morego 30, 16163, Genova, Italy, roberto.marotta@iit.it.

⁵ Medical Physics, Centre for Cardiovascular Science, University of Edinburgh, 47 Little France Crescent, EH16 4TJ, Edinburgh, United Kingdom, carmel.moran@ed.ac.uk.

Corresponding Authors

* Federica Rinaldi, Department of Drug Chemistry and Technology, Sapienza University of Rome, Piazzale A. Moro 5, 00185, Rome, Italy, federica.rinaldi@uniroma1.it.

1
2
3
4 * Elena Del Favero, Department of Medical Biotechnologies and Translational Medicine,
5
6 University of Milan, Via Fratelli Cervi 93, 20090, Segrate, Italy, elena.delfavero@unimi.it. (Orcid:
7
8 0000-0002-6584-1869)
9

10
11
12 ‡ These authors contributed equally. (Patrizia Nadia Hanieh‡, Caterina Ricci‡)
13
14

15 **Competing Interests**

16
17
18
19 The authors declare the following competing financial interest(s): The authors Federica Rinaldi,
20
21 Carlotta Marianecchi, Maria Carafa and Andrea Bettucci are inventors of a patent on the
22
23 nanobubbles used in the present research. The other co-authors have no conflict of interest.
24
25
26

27 **Word count for abstract:** 150
28
29

30
31 **Complete manuscript word count** (including body text and figure legends, but excluding
32
33 abstract, title page, and references), 4907
34
35

36 **Number of references:** 34
37
38

39
40 Number of figures/tables: 8
41
42

43 **ABSTRACT**

44
45
46
47 Nanoscale echogenic bubbles (NBs), can be used as a theranostic platform for the localized
48
49 delivery of encapsulated drugs. However, the generation of NBs is challenging, because they have
50
51 lifetimes as short as milliseconds in solution. The aim of this work has been the optimization of a
52
53 preparation method for the generation of stable NBs, characterized by measuring: a) acoustic
54
55 efficiency, b) nano-size, to ensure passive tumour targeting, c) stability during storage and after
56
57 injection d) ability to entrap drugs. NBs are monodisperse and ultra-stable, their stability achieved
58
59
60
61
62
63
64
65

1
2
3
4 by generation of an amphiphilic multilamellar shell able to efficiently retain the PFC gas. The NBs
5
6 perform as good acoustic enhancers over a wide frequency range and out of resonant conditions,
7
8 as tested in both *in vitro* and *in vivo* experiments, proving to be a potential platform for the
9
10 production of versatile carriers to be used in ultrasound-assisted diagnostic, therapeutic and
11
12 theranostic applications.
13
14

15 16 17 18 **KEYWORDS**

19
20
21 Nanobubbles, ultrasound contrast agents, acoustics, theranostics, drug delivery
22
23
24
25
26
27

28 **Introduction**

29
30
31 Microbubbles, comprising a gas core and stabilizing outer shell, have been used in diagnostic US
32
33 imaging as contrast agents (UCA) since the early 1990s after it was demonstrated that an outer
34
35 shell extended the bubble lifetime *in vivo* (1). The enhancement of the ultrasound signal is a result
36
37 of the acoustic impedance mismatch between the microbubbles and the surrounding medium.
38
39 Recently, the potential role of such microbubbles as theranostic drug delivery systems has also
40
41 been the focus of much research (2).
42
43
44

45
46
47 At present, the UCAs approved for clinical use by FDA are relatively few: Optison (GE Healthcare
48
49 Inc, Princeton, NJ, USA) and Definity (or Luminity, Lantheus Medical Imaging, Inc N. Billerica,
50
51 MA, USA), enclosing perfluoropropane (C₃F₈); and Lumason (or SonoVue, Bracco Imaging SpA,
52
53 Milan, Italy) enclosing sulfur hexafluoride (SF₆) (3). Sonazoid, enclosing perfluorobutane (C₄F₁₀),
54
55 is used in Asia and Norway for liver and breast imaging (4).
56
57
58
59
60
61
62
63
64
65

1
2
3
4 Due to their size (1 - 5 μm), MBs cannot extravasate from intravascular into interstitial space.
5
6 Consequently, in a clinical setting, the US contrast agents are used to qualitatively assess vascular
7
8 perfusion defects and, by their dynamic enhancement, to provide differential diagnosis of organ
9
10 abnormalities (5). On the other hand, pilot work has shown that by functionalization of the MBs
11
12 shell, MBs may have the potential to differentiate between malignant and benign tumors (6) and
13
14 there has been increasing interest in the potential of MBs as integrated systems for theranostic
15
16 applications, with drugs encapsulated within the microbubble structure (7). Real-time monitoring
17
18 of the bubbles could be achieved by non-destructive US detection, and subsequent drug release
19
20 could be triggered by higher-pressure US, with localized therapeutic impact. Preclinical *in vivo*
21
22 studies incorporating chemotherapeutics have shown encouraging results while lowering the
23
24 impact of adverse effects (8-10). Nonetheless, the size of MBs remains one of the major
25
26 limitations, as tumour targeting requires crossing the permeable tumour vessel walls, with vascular
27
28 endothelial gaps in the size-range of hundreds of nanometers.
29
30
31
32
33
34

35
36 Nano-sized bubbles (NBs) can potentially overcome this impasse as they can extravasate and enter
37
38 tumour tissue (11). Once there, NBs could accumulate via the enhanced permeability and retention
39
40 effect (12), promoting efficient uptake either directly or by drug-release stimulated by an US field.
41
42 However, this promising application poses additional constraints to the design of bubble systems
43
44 with appropriate structure and *in vivo* high performance.
45
46
47
48

49
50 The generation of NBs is challenging, and indeed whether NBs can exist is a source of controversy
51
52 in the literature. Nano-sized bubbles are considered significantly more unstable than micro-sized
53
54 bubbles, and their lifetime can be as short as milliseconds before they dissolve into the solution
55
56 (13). The use of hydrophobic gases, such as C_3F_8 or SF_6 , is expected to slow down the gas leakage
57
58 from NBs (14), further improving the bubble longevity with heavier perfluorocarbons (PFCs), such
59
60
61
62
63
64
65

1
2
3
4 as C₄F₁₀, C₅F₁₂, and C₆F₁₄. However, the high boiling temperature of these PFCs and the NBs-
5
6 associated Laplace pressure, may lead to the formation of nanodroplets, with liquid- rather than
7
8 gas-core, at physiological temperature. Indeed, several studies describe a strategy, based on the
9
10 formulation of nanodroplets, with a liquid core undergoing a liquid-to-vapour transition when
11
12 exposed *in situ* to an intense acoustic pulse (acoustic droplet vaporization) (15, 16). Nanodroplets
13
14 can extravasate into interstitial spaces before activation, while the “activated” bubbles can be used
15
16 for both diagnostics and drug delivery. However, there are limitations to this technology – until
17
18 they are activated, nanodroplets cannot be visualized by US imaging; significant acoustic pressures
19
20 are required to initiate droplet vaporization; and bubbles formed *in situ* by acoustic vaporization,
21
22 tend not to be in the sub-micron range, but rather micro-bubbles.
23
24
25
26
27
28

29
30 The possibility to generate stable NBs for theranostic application is therefore a topic of great
31
32 interest. Several studies suggest that long-lived nano-sized bubbles can exist (13, 17, 18), although
33
34 whether the ‘bubbles’ are gas-filled, nanodroplets or nanoparticles continues to be a challenging
35
36 issue (19).
37
38
39

40 The proposed protocols to produce lipid-shell NBs are similar to those employed for MBs
41
42 production. A key factor in the manufacture and stability of NBs is the presence of an interfacial
43
44 shell (20), where phospholipids, proteins, or polymers may help in reducing the interfacial tension,
45
46 extending the life of nanobubbles (21). Precise shell engineering can improve nanobubble stability
47
48 and provide a level of resilience to mechanical deformations induced by ultrasound insonation or
49
50 during circulation (18). The selection of the composition and formation of the interfacial envelope,
51
52 together with the choice of enclosed gas, is of importance to obtain diagnostically and
53
54 therapeutically useful NBs (22, 23).
55
56
57
58
59
60
61
62
63
64
65

1
2
3
4 The aim of this paper is to describe the design and construction of a NBs platform for both drug
5 delivery and echogenic signal enhancement. NBs were prepared and characterized exhaustively
6 with respect to the following key-enabling properties: a) acoustic efficiency, b) nano-size, to
7 ensure passive tumour targeting, c) stability during storage and after tail vein injection d) ability
8 to entrap lipophilic and hydrophilic drugs. Two types of NBs were manufactured using this
9 platform - innovative surfactant NBs and phospholipid-based NBs. Both types of nanobubbles
10 were filled with PFC gas, that is biocompatible, inert, and chemically highly stable and is not
11 metabolized in the body after injection (24).
12
13
14
15
16
17
18
19
20
21
22
23

24 The physical-chemical characterization of the systems was performed by combining
25 complementary experimental techniques. Static and Dynamic Light Scattering (SLS, DLS),
26 fluorescence spectroscopy, shelf-life and biological stability studies, combined with Small-Angle
27 X-ray scattering (SAXS) and cryo-electron (CryoEM) tomography experiments, were used to
28 unravel the multilayer structure of the NBs, to test their resistance to stress and deformation and
29 to determine their stability during their notably extended shelf-life. Acoustic measurements *in*
30 *vitro* and in a pilot *in vivo* study demonstrated acoustic enhancement of the nanobubbles compared
31 to a commercial microbubble product.
32
33
34
35
36
37
38
39
40
41
42
43

44 **Methods**

45
46
47
48 1,2-dimyristoyl-sn-glycero-3-phosphocholine (DMPC) was from Avanti Polar Lipids (Alabaster,
49 Alabama, USA). Dicaprylyl phosphate (DCP), Sorbitan monolaurate (Span20), cholesterol (Chol),
50 HEPES salt {N-(2-hydroxyethyl) piperazine-N'-(2-ethanesulfonic acid)}, pyrene, diphenylhexatriene
51 (DPH), calcein, Nile Red, human serum (HS), bovine serum (BS), tetradecafluorohexane (PFC)
52
53
54
55
56
57
58
59
60
61
62
63
64
65

1
2
3
4 were from Sigma–Aldrich (Milan, Italy). Sonovue[®] was generously gifted by Bracco (Milan,
5
6 Italy).

7
8
9
10 Phospholipid-based or surfactant-based vesicles were prepared by thin-film hydration method.
11
12 Details in the Supplementary Material.
13
14

15 **Experimental techniques**

16 **Structural characterization**

17
18
19
20
21
22 Static and dynamic laser light scattering (SLS), ζ -potential and density measurements were
23
24 performed on samples at 25°C.
25
26

27
28 Cryo Transmission Electron Microscopy (Cryo-TEM) and cryo-electron tomography images were
29
30 acquired on frozen hydrated samples of NBs using a Tecnai G2 F20 microscope (FEI company,
31
32 the Netherlands). Computation of tomograms and postprocessing were performed using the IMOD
33
34 4.9.2 software package (25).
35
36

37
38
39 Small Angle X-Ray Scattering (SAXS) measurements were performed at the ID02 high-brilliance
40
41 beamline at the ESRF Synchrotron (Grenoble, France). From the SAXS intensity spectra,
42
43 information on the size, shape and internal structure of the particles in solution could be obtained.
44
45 Data fitting was performed with the SaSView application (version 4.2.0, 2019) (26) with a core
46
47 multi-shell spherical model.
48
49

50
51
52 Bilayer fluidity of NBs was evaluated by using the hydrophobic probe 1,6-diphenyl-1,3,5-
53
54 hexatriene (DPH) (27). In parallel, bilayer polarity and microviscosity were determined by
55
56 fluorescence experiments on NBs loaded with Pyrene, used to detect the lateral distribution and
57
58 mobility of the enveloping membrane compounds.
59
60
61
62
63
64
65

1
2
3
4 Experimental details in the Supplementary Material.
5
6

7 **Pulse-echo and Photoacoustic analysis**

8
9

10 In order to test the shelf stability of the NBs, a pulse-echo technique was used to determine the
11 acoustic behavior of the NBs at different concentrations and time-points after preparation. The
12 presence of the gas inside NBs was confirmed by the photoacoustic technique (28). Details on the
13 experiments in the Supplementary Material.
14
15
16
17
18
19
20

21 **NBs stability and probe-loading studies**

22
23

24 The time stability of NBs, stored at room temperature and $T = 4^{\circ}\text{C}$ up to 90 days, and upon contact
25 with human serum or bovine serum up to 45% (over 3 hours at $T = 37^{\circ}\text{C}$) was evaluated, by
26 determining the average size and ζ -potential.
27
28
29
30
31
32

33 The presence of inner gas in the NBs was tested by acoustic attenuation measurements (after 90
34 days at 4°C) and SAXS measurements (after 30 days at 4°C).
35
36
37
38

39 In order to check the ability of NBs to entrap drugs and gas, simultaneously, fluorescent probes,
40 namely, Calcein and Nile Red, as models for hydrophilic and hydrophobic molecules, respectively,
41 were both included within the NBs during preparation. Loaded NBs were characterized in terms
42 of acoustic efficiency, entrapment efficiency, size and ζ -potential in comparison to unloaded NBs.
43
44
45
46
47
48

49 **Echographic studies**

50
51

52 The small animal imaging studies were carried out in accordance with the UK Home Office
53 Animals (Scientific Procedures) Act, 1986 and the European Committees Council Directive of
54 November 1986 (86/609/EEC) and were assessed by the University of Edinburgh Ethical Review
55 Committee. Details on the experiment are reported in the Supplementary Material.
56
57
58
59
60
61
62
63
64
65

1
2
3
4
5
6
7
8 **Results and Discussion**
9

10 **Preparation of NBs**
11

12
13
14 As the first and crucial step (17, 29, 30), we focused on the protocol for the production of stable
15
16 NBs. The optimization of the NBs fabrication protocol constitutes the first result of this work. A
17
18 set of experimental techniques were applied to assess that the preparation procedure led to the
19
20 effective formation of NBs upon internalization of the gas into closed amphiphilic shells, hereafter
21
22 called vesicles, either phospholipid- or surfactant-based.
23
24

25
26
27 NBs were prepared by using different phospholipids and surfactants, together with cholesterol
28
29 (Chol), in different molar ratio. The sonication parameters and the technique of gas supply were
30
31 the critical factors in the formation of the NBs.
32
33

34
35 Liquid PFC was added with a syringe to a vesicular dispersion, at room temperature, and submitted
36
37 to sonication for 15 minutes, with an ultrasound generator equipped with a microprobe operating
38
39 at 20 kHz, with amplitude of 16% (Vibracell-VCX 400-Sonics, USA). During sonication,
40
41 temperature increased to 70°C. Then the nanobubbles dispersion was cooled by thermal shock in
42
43 melting ice, for 10 minutes. Care was taken to avoid PFC loss by sealing the container. As a final
44
45 step, the NBs were purified at 25°C by centrifugation in a MPW-260R (MPW Med. Instruments)
46
47 at 600 rpm for 20 minutes.
48
49
50
51

52
53 Finally, the low-HLB Span20 surfactant and the phospholipid DMPC, also in association with the
54
55 anionic surfactant DCP, were chosen as the most effective constituents in the formation of NBs
56
57 (Table S1).
58
59
60
61
62
63
64
65

The final gas volume concentration was derived by calculating the mean internal volume of the bubbles at a given surfactant concentration. The external size of the bubbles and the thickness of their shell were obtained from DLS and SAXS results. Given the polydispersity in bubbles size and shell thickness, an indicative estimate of the gas concentrations in the final suspensions gives about 20 mm³/ml for phospholipid-based NBs and 6 mm³/ml for surfactant-based NBs, which is comparable to the commercial SonoVue (Bracco) formulation (8 mm³/ml, as stated by the manufacturer).

General suitability of NBs

NBs were submitted to a range of experimental tests to verify their structural and acoustic properties.

The populations of NBs were quite monodisperse ($PDI \leq 0.2$) with 150-175 nm mean size (Table 1). The ζ -potential ranged from weakly negative for DMPC-based NBs to markedly negative for Span20-based NBs (-42 ± 2 mV). The addition of 24.7 mM of the anionic surfactant DCP conferred a higher negative ζ -potential (-71 ± 2 mV).

Sample	Size (nm) ± SD	ζ -potential (mV) ± SD	PDI	Fluidity (Anisotropy)	Polarity (I ₁ /I ₃)	Microviscosity (I _E /I ₃)
DMPC NBs	151 ± 3	-4 ± 1	0.20	0.25	1.05	0.44
DMPC-DCP NBs	130 ± 2	-71 ± 2	0.20	0.24	1.07	0.43
Span20 NBs	173 ± 4	-42 ± 2	0.12	0.24	0.95	0.3

Table 1. Size (DLS), charge (ζ -potential) and bilayer characterization in terms of fluidity (anisotropy measurements) and polarity and microviscosity (Pyrene fluorescence spectra

1
2
3
4 evaluation) of different NBs. Listed values are determined as the mean \pm standard deviation of n
5 = 3 NBs sample measurements.
6
7
8
9

10
11 The crucial test was to verify the presence of a gas core inside the NBs, which was performed by
12 density, static light scattering (SLS) and acoustic analysis.
13
14

15
16
17 The density of NBs suspensions was measured in the temperature range 20–70 °C and compared
18 with the density of the corresponding vesicles at the same lipid and surfactant concentration
19 (Supplementary Material, Table S2). At 20 °C, the density of vesicles and NBs suspensions is
20 higher than that of the solvent. This is due to the density of amphiphiles (and higher for Span20)
21 and in the case of NBs suggests the possible coexistence in the core of Perfluorohexane in the gas
22 phase (density about 0.01 g/cm³) and in the liquid phase (density 1.7 g/cm³). Interestingly, the
23 temperature dependence of the density is clearly different for systems with or without PFC, as
24 reported in Figure 1.
25
26
27
28
29
30
31
32
33
34
35
36
37
38
39
40
41
42
43
44
45
46
47
48
49
50
51
52
53
54
55
56
57
58
59
60
61
62
63
64
65

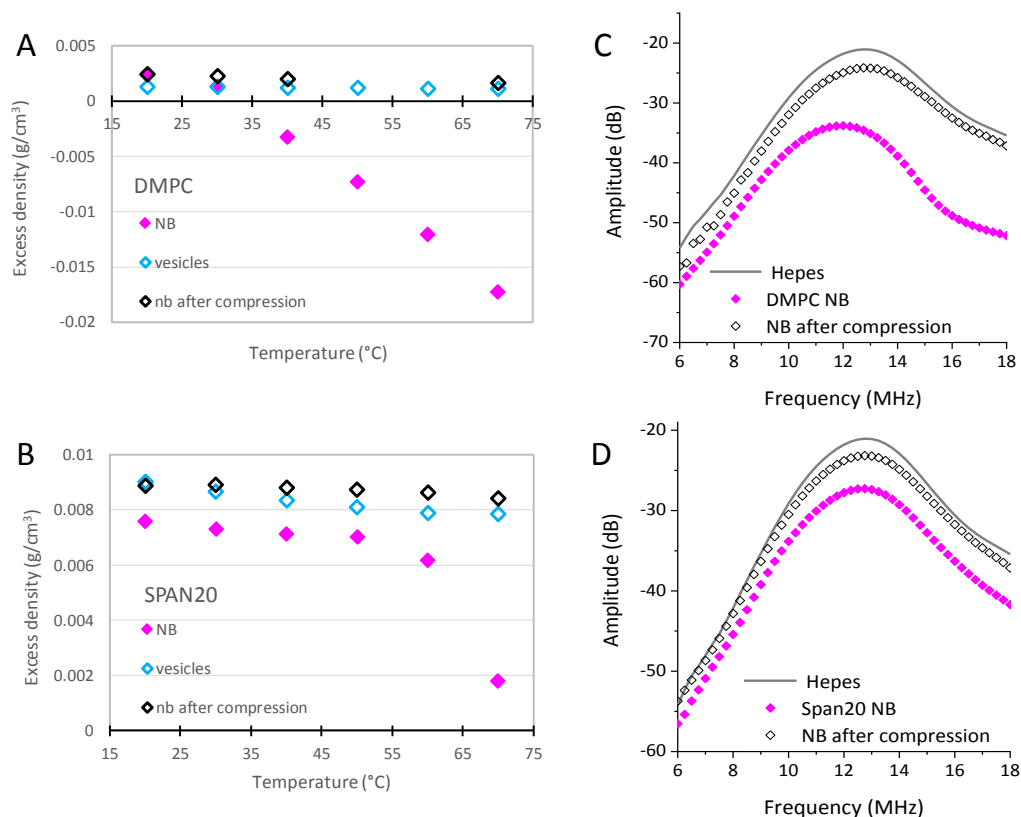


Figure 1. Excess density of samples with respect to water at different temperatures, Panel A DMPC, Panel B Span20. Amplitude of the ultrasound signal after traversing the test-cell over the frequency range 6-18 MHz, DMPC Panel C, Span20 Panel D. The amplitude of the ultrasound signal measured for the solvent (Hepes) is reported for comparison.

The density of the DMPC-based vesicles suspension decreases slightly as temperature is raised. Reversely and notably, the density of the DMPC-based NBs dispersion hugely decreases and between 30°C and 40 °C it is already lower than the solvent water. This result stems from the presence of gas in the NBs at physiological temperatures, well below the boiling point of Perfluorohexane (bp = 56.6 °C).

1
2
3
4 For the Span20-based systems, while the density of the vesicle solution slightly declines as
5
6 temperature is raised, that of NBs steeply drops at temperatures higher than 50 °C, as reported in
7
8 Figure 1 Panel B.
9

10
11
12 To further test the presence of gas in NBs at physiological temperatures, below 40 °C, all
13
14 suspensions were submitted to external mechanical compression, directly in the cell of the density
15
16 meter ($\Delta p = 2 \times 10^5 \text{ N/m}^2$), and then, once compression had been released, their density was
17
18 measured again. The density of vesicle suspensions is not affected by compression, as expected
19
20 for an amphiphilic shell enclosing an incompressible aqueous core. Conversely, the density of the
21
22 NBs suspensions is dramatically altered after compression, both in absolute values and in the
23
24 temperature dependence, becoming similar to the parent vesicles (Panel A and B, Figure 1). This
25
26 finding suggests that the increase of external pressure disturbed the NBs shells inducing their
27
28 shrinkage and then the leakage of the gas.
29
30
31
32
33
34

35 Moreover, vesicles and NBs were observed by SLS at $T = 25 \text{ °C}$. The intensity scattered from NBs
36
37 is 10-fold the one from the corresponding vesicles at the same concentration (Supplementary
38
39 Material, Table S3). This significant difference cannot be attributed only to the 20% different size,
40
41 but rather depends on a higher contrast of NBs (see Methods), suggesting that gas-PFC is enclosed
42
43 in NBs even at 25°C.
44
45
46
47

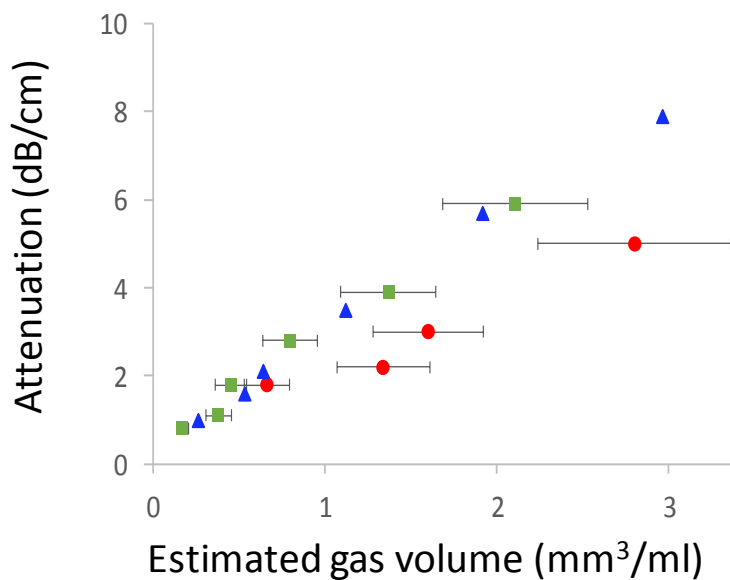
48 In parallel, the acoustic efficiency of NBs was measured by a pulse-echo technique before and
49
50 after mechanical compression ($\Delta p = 2 \times 10^5 \text{ N/m}^2$).
51
52
53

54 Results (Figure 1, Panel C and Panel D) clearly show that the considerable efficiency of both
55
56 DMPC-based and Span20-based NBs in attenuating the US beam vanishes after compression,
57
58 becoming similar to that of the buffer.
59
60
61
62
63
64
65

1
2
3
4 The presented set of results, obtained with complementary techniques, confirms the actual
5 presence of gas-phase-PFC inside the NBs, also in the 25-40 °C temperature range. Inside the NBs,
6 the gas-PFC is probably in equilibrium with a small volume of liquid-PFC and is trapped and
7 stabilized by a closed shell built by the amphiphilic molecules, which is capable of withstanding
8 the overpressure of curvature without collapsing.
9
10
11
12
13
14

17 **Acoustic efficiency**

20 The acoustic efficiency of the NBs was evaluated with a pulse-echo technique and compared to
21 one of SonoVue[®]. Figure 2 shows the attenuation of the incident acoustic beam at 14 MHz for
22 DMPC NBs, Span20 NBs and SonoVue[®] microbubbles systems, as a function of concentration,
23 expressed as estimated gas concentration. The central frequency of the ultrasound transducer (14
24 MHz) is out of the resonance range for both the SonoVue[®] (about 2.5 MHz (31)) and NBs (higher
25 than 20 MHz, see Figure S1, Supplementary Material).
26
27
28
29
30
31
32
33
34
35
36
37



1
2
3
4 **Figure 2.** Acoustic attenuation at 14 MHz for Span20 NBs (green squares), DMPC NBs (red dots)
5 and SonoVue MBs (blue triangles) in Hepes buffer at different estimated gas concentrations
6 vol/vol (error bar $\pm 20\%$, for SonoVue the gas content is stated by manufacturer).
7
8
9

10
11
12
13
14 As expected, and reported in Figure 2, acoustic attenuation increases almost linearly with
15 concentration for both NBs preparations. The attenuation values are comparable for NBs and
16 SonoVue[®] at similar estimated gas concentration. In addition, for Span20 NBs, the frequency
17 spectra of the US signal attenuation, at different concentrations, are reported in Figure S1,
18 Supplementary Material, showing similar attenuation efficiency across the analyzed frequency
19 range (6-20 MHz).
20
21
22
23
24
25
26
27
28

29 The efficiency of gas trapping within the NBs was also evaluated using a photoacoustic cell and
30 the results were compared with those obtained for SonoVue[®] (Figure S2, Supplementary Material).
31
32 Dampening of the vibration amplitudes for the first and second resonance frequencies of the
33 photoacoustic cell confirm that NBs and SonoVue[®] are comparable for gas trapping and acoustic
34 performance.
35
36
37
38
39
40
41

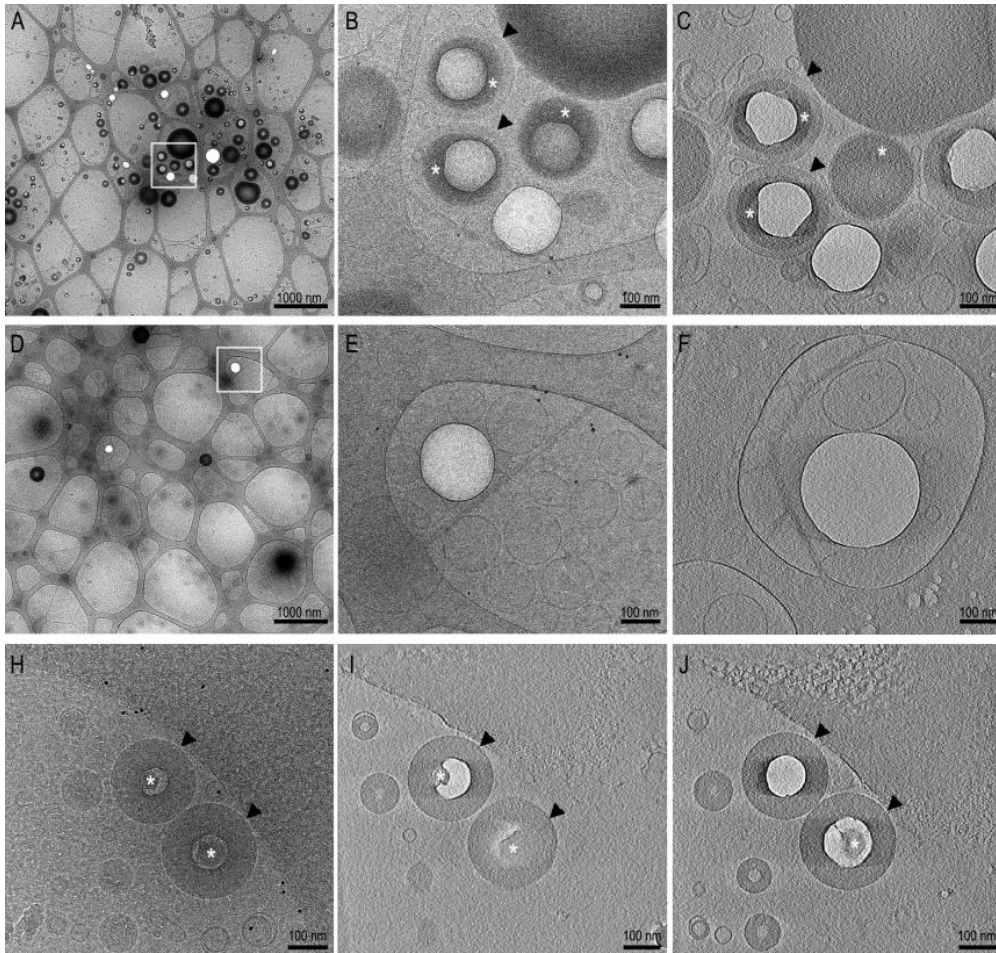
42 **Morphology and internal structure of NBs**

43
44

45 The morphology and the internal structure NBs can affect the volume of encapsulated gas and their
46 stability both in *in vitro* and *in vivo* conditions. A detailed investigation of the morphology and
47 structure of the NBs was performed by Cryo-EM, SAXS and fluorescence analyses.
48
49
50
51
52
53

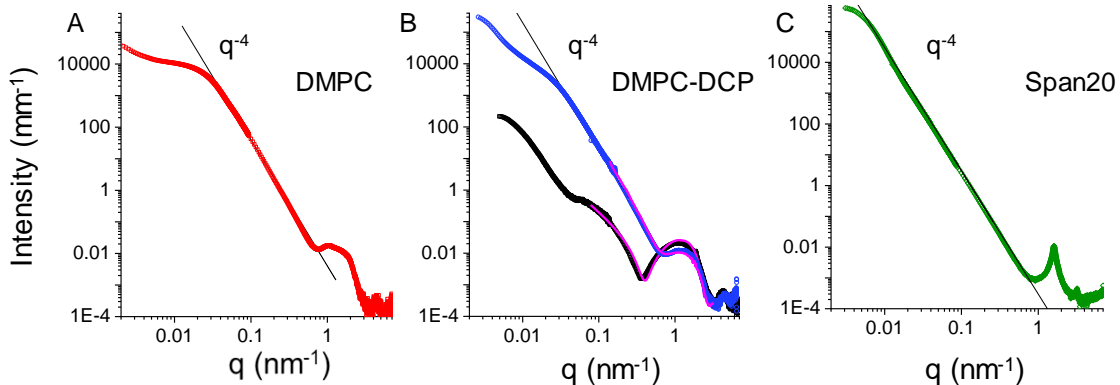
54 CryoEM projection images and cryo electron tomographies revealed that all samples contain
55 subspherical nanobubbles with a characteristic electron-transparent gas-enriched core (see Figure
56 3). In DMPC-based NBs, most particles have a multilamellar envelope, but some nanoparticles are
57
58
59
60
61
62
63
64
65

1
2
3
4 unilamellar (see Figure 3, top row, A-C). Some electron-dense diffuse material, probably liquefied
5 gas, is present between the membrane and the gaseous core in many nanoparticles (see Figure 3,
6
7
8
9 B-C). The morphology of DMPC-DPC-based nanoparticles is not significantly different (see
10
11
12 Figure 3, central row, D-F). Conversely, the Span20 NBs sample contains nanoparticles with
13
14 distinctive and different morphology. A thick and massive shell surrounds the electron transparent
15
16 core, suggesting that the envelope is likely to have a multi-lamellar structure (see Figure 3, bottom
17
18 row, H-J). Also in this system, some irregular electron-dense material, again probably liquefied
19
20 gas, is visible inside the core itself. Finally, in all samples we observed several nanoparticles
21
22 devoid of gas and many vesicles, that could either be present in the formulations or partially
23
24 devoid of gas and many vesicles, that could either be present in the formulations or partially
25
26 emptied during rapid freezing.
27
28



1
2
3
4
5
6
7
8 **Figure 3.** Cryo-EM and cryo-tomography. Top row, DMPC-based NBs: A) low magnification
9 projection image of vitrified sample; B) higher magnification of the region boxed in A; C)
10 tomographic slice (10 averaged sections) showing DMPC NBs. Central row, DMPC-DPC-based
11 NBs: D) low magnification projection image of vitrified sample; E) higher magnification of the
12 region boxed in D; F) tomographic slice (10 averaged sections) showing DMPC-DPC NBs.
13 Bottom row, Span 20-based NBs: H) high magnification of particles; I) and J) are different
14 tomographic slices (10 averaged sections) showing Span20 NBs. Black arrowheads and white
15 asterisks point respectively to multi-lamellar membranes and electron-dense regions.
16
17
18
19
20
21
22
23
24
25
26
27
28
29
30
31
32
33
34
35

36
37 The structure of the various NBs was assessed by SAXS. The analysis of the intensity spectra
38 measured for NBs, reported in Figure 4, reveals interesting structural features and confirms the
39 presence of a gas core.
40
41
42
43
44
45
46
47
48
49
50



51
52 **Figure 4.** SAXS intensity spectra for different NBs. A) DMPC (red), B) DMPC-DPC (blue), C)
53 Span20 (green). Straight black lines draw the decay behavior $I(q) \div q^{-4}$, characteristic of hard
54 interfaces between two physical media. The spectrum of a simple water-enclosing DMPC-DPC
55 closed bilayer (black) is also shown in panel B for comparison with the corresponding gas-
56 enclosing DMPC-DPC NBs, together with the bilayer fits (magenta).
57
58
59
60
61
62
63
64
65

1
2
3
4
5
6
7
8 For ease of discussion, we report the intensity profile of DMPC-DCP NBs together with that of
9 DMPC-DCP vesicles (Figure 4B). Differences are clearly visible in the $q < 1 \text{ nm}^{-1}$ region, revealing
10 primary features of the overall particles. The scattered intensity at low- q is orders of magnitude
11 higher for DMPC-DCP NBs than for vesicles. This result confirms the presence of gas inside the
12 NBs, as the scattered intensity is proportional to the square of the difference in electron density
13 between the particles, and in particular of their gas core and the solvent. Also, the intensity decay
14 is much steeper for NBs. The straight black line drawn on top of the experimental spectrum follows
15 a decay behavior of $I(q) \div q^{-4}$, which is characteristic of hard interfaces between two physical
16 media (32). This reveals that the interface between the gas core and the surrounding stabilizing
17 DMPC-DCP shell is well defined, as expected for gas bubbles in water. Similar comparison is
18 shown for all NBs in Figure S3, Supplementary Material, and the same observations are applicable
19 for all the investigated systems. Deviation from the q^{-4} decay below $q = 0.05 \text{ nm}^{-1}$ indicates that
20 the size of the nanobubbles is of the order of hundreds of nanometers, in agreement with DLS
21 results.

22
23
24
25
26
27
28
29
30
31
32
33
34
35
36
37
38
39
40
41
42 On the local length-scale, the structure of NBs is reflected in the features of the intensity spectra
43 at $q > 0.1 \text{ nm}^{-1}$. An identical form factor of a single closed lipid bilayer, about 5 nm thick, has been
44 used to model both the external shell of DMPC-DCP vesicles and of NBs. In the NBs an inner gas
45 core replaces the water core of vesicles (electron density profiles are reported in Figure S4,
46 Supplementary Material). We suggest that an additional lipid monolayer is present at the PFC-
47 water interface, allowing for the stabilization of the gas-in-liquid nanobubble. The enclosing lipid
48 lamellar shell, can constitute a good barrier against PFC diffusion.
49
50
51
52
53
54
55
56
57
58
59
60
61
62
63
64
65

1
2
3
4 DMPC NBs display a local structure very similar to that of DMPC-DCP NBs, particles being
5 enclosed by a bilayer of lipids. A fraction of multilamellar shells is present, as inferred by the small
6
7 characteristic peak around 1 nm^{-1} . The formation of multilamellar shells is expected for lipids with
8
9 low charge.
10
11

12
13
14 Span20 NBs gives rise to quite a different intensity spectrum, shown in Figure 4D. Bragg peaks at
15
16 $q = 1.6 \text{ nm}^{-1}$ and 3.2 nm^{-1} emerge, corresponding to a characteristic repeat distance inside the
17
18 particle of 3.8 nm, interestingly, roughly twice the length of a Span20 molecule. Exactly the same
19
20 structure peaks are observed for the Span20 vesicles (see Figure S3, Supplementary Material) as
21
22 already reported (33). In the Span20 NBs the gas core is surrounded by a multilayered shell made
23
24 of stacked adjacent bilayers without interlamellar water, thus detailing the CryoTEM observation
25
26 of a thick and massive shell.
27
28
29
30

31
32 The presence of unilamellar or multilamellar enveloping shells can be a key parameter both for the
33
34 stability of the NBs and for the efficiency in the encapsulation of both hydrophobic and hydrophilic
35
36 drugs, in view of their use as drug delivery systems.
37
38
39
40

41 To evaluate the propensity of NBs to host and then release entrapped drugs, the NBs shell fluidity,
42
43 polarity and microviscosity have been measured. Results show that NBs are equipped with bilayers
44
45 with average values of fluidity, microviscosity and polarity, useful to entrap, retain and then release
46
47 lipophilic drugs (34) (Table 1). The parent vesicles show identical values (Table S4,
48
49 Supplementary Material) confirming the encapsulation of the gas totally in the inner compartment
50
51 of NBs, without influencing bilayer features.
52
53
54
55

56 **Stability of NBs**

57
58
59
60
61
62
63
64
65

1
2
3
4
5
6
7
8
9
10
11
12
13
14
15
16
17
18
19
20
21
22
23
24
25
26
27
28
29
30
31
32
33
34
35
36
37
38
39
40
41
42
43
44
45
46
47
48
49
50
51
52
53
54
55
56
57
58
59
60
61
62
63
64
65

The NBs morphology, structure and physico-chemical properties are promising for the development of a commercial product to be used in diagnostics or theranostics. For this purpose, the Span20 NBs display the most favorable combination of features (small size, multi-layered shell), that have to be paralleled by good storage and biological stability.

Shelf-life stability of Span20 NBs was assessed checking particle size and surface charge over 3 months at two different storage temperatures, and SAXS profiles were also taken at 30 days' post-preparation. Parallel investigation was performed on DMPC NBs, for comparison. In Figure 5, NBs behavior upon storage is presented.

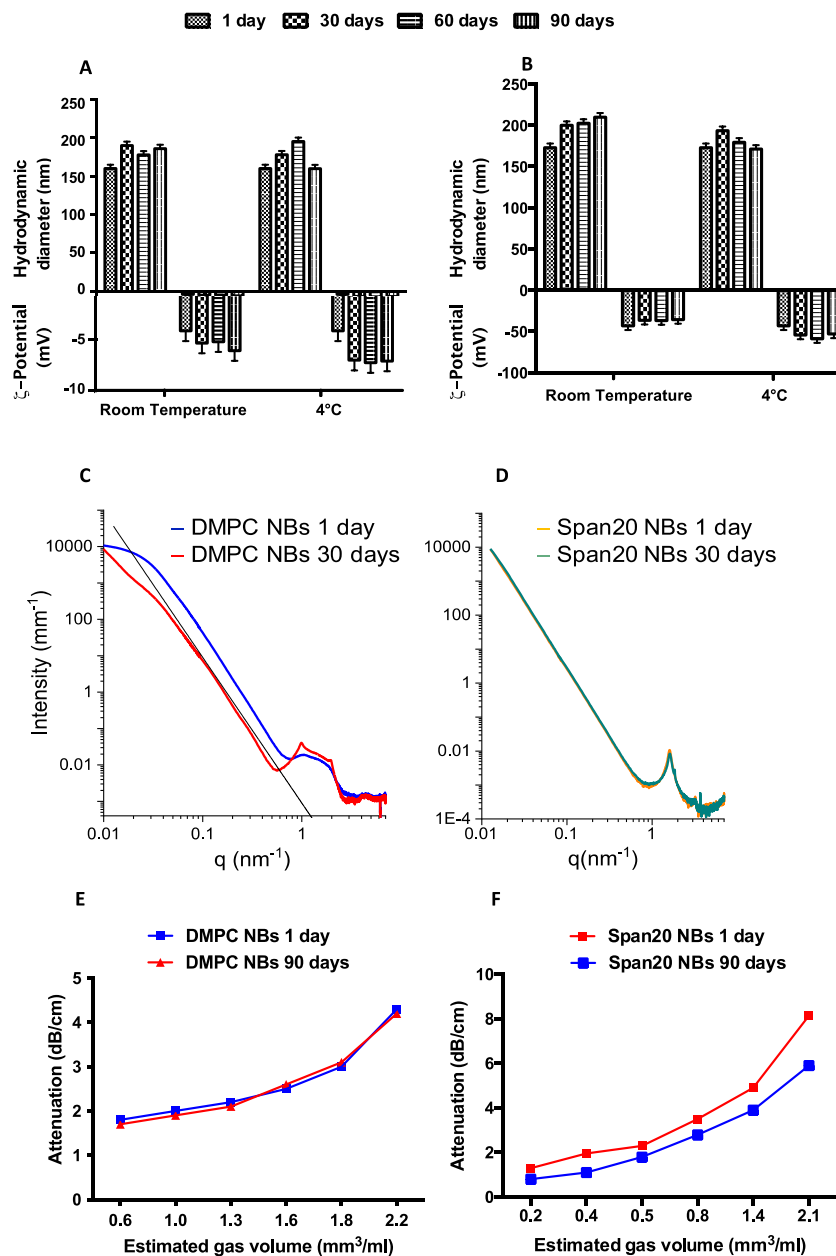


Figure 5. Time stability of DMPC NBs (left column) and Span20 NBs (right column). A), B): hydrodynamic diameter and ζ -potential, up to 90 days at two different storage temperatures (RT and 4°C). C), D): comparison of SAXS intensity spectra taken at preparation and after 30 days of storage. E), F): ultrasonic (14 MHz) attenuation of NBs diluted in HEPES buffer at different estimated gas concentrations, at preparation and after 90 days of storage.

1
2
3
4 NBs are stable with respect to size and charge up to 90 days at both storage temperatures. Also,
5
6 their internal structure is preserved, as tested by SAXS measurements performed after 30 days.
7
8
9 Span20 NBs are particularly stable, showing both the same internal structure and total volume
10
11 fraction (Figure 5, Panel D). Notably, NBs maintain their acoustic properties almost unchanged
12
13 after 90 days' storage (Figure 5, panel E and F).
14
15

16
17 Overall, the novel NBs presented here display outstanding stability (size and ζ -potential,
18
19 persistence of acoustic signal and gas retention), significantly better than commercial products.
20
21 For example, SonoVue[®] solution, prepared according to the manufacturer's specifications, was
22
23 found to lose its acoustic properties in approximately 4 days, as evaluated by pulse-echo and
24
25 photoacoustic measurements (Supplementary Material, Figure S5).
26
27
28
29

30
31 As for the biological stability of NBs, it has been tested at temperatures up to 40 °C. In Figure S6,
32
33 Supplementary Material, data related to hydrodynamic diameter and ζ -potential before experiment
34
35 and after contact with 45% (v/v) human serum (time 0-3 hours) are reported. NBs display good
36
37 stability, at least 180 minutes. Stability was tested also in bovine serum (Figure S7, Supplementary
38
39 Material) with similar results.
40
41
42
43
44
45
46

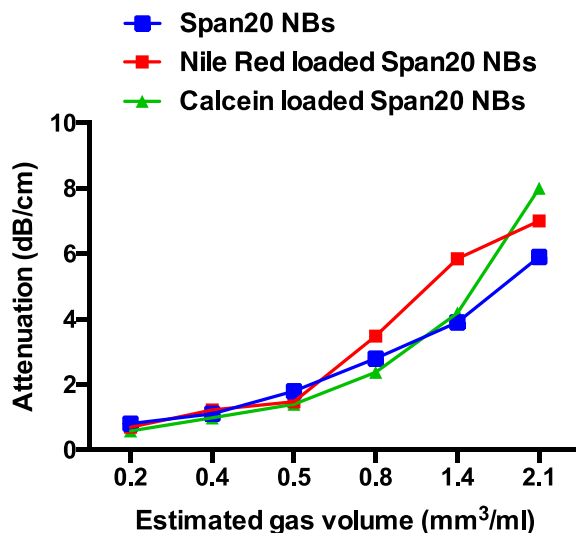
47 **NBs as a putative theranostic platform: drug-gas co-loading and *in vivo* pilot-testing**

48
49

50 The long time stability and persistence of the NBs even in serum emerges as a prominent property
51
52 of the novel NBs presented here. In particular, Span20 NBs display the best performance in terms
53
54 of size, stability, prolonged gas retention and acoustic properties. These features support their
55
56 application as a multipurpose platform, both as new contrast media and as drug carriers, via the
57
58 co-loading of gas and drugs, suitable for controlled release. To investigate the potential of NBs as
59
60
61
62
63
64
65

1
2
3
4 a dual diagnostic and theranostic platform, Span20 NBs were submitted to further investigation to
5
6 explore their potential for drug loading and *in vivo* use.
7
8

9
10 Span20 NBs were loaded with two fluorescent probes, the hydrophilic calcein and the hydrophobic
11 Nile Red, as mimics of small drugs. Their presence in Span20 NBs was checked by measuring
12 their fluorescent signals (Table S5, Supplementary Material). Moreover, amplitude attenuation
13 results reported in Figure 6, show that the co-loading of gas and drug mimics maintains the acoustic
14 efficiency of the NBs.
15
16
17
18
19
20
21
22



23
24
25
26
27
28
29
30
31
32
33
34
35
36
37
38
39
40
41
42
43 **Figure 6.** Ultrasonic (14 MHz) attenuation of Span20 NBs, without (blue) and loaded with
44 fluorescent probes (red and green), upon dilution in Hepes buffer at different estimated gas
45 concentrations with respect to the prepared formulations.
46
47
48
49
50
51

52
53 Notably, it appears that the thick multilayered envelope of Span20 NBs sustains their ability to
54 efficiently solubilize both hydrophilic and hydrophobic drugs with relatively low impact on their
55 stability and echogenicity. In fact, the peculiar tightly layered structure of Span20 NBs shell
56
57 provides the opportunity to efficiently solubilize hydrophobic compounds in the lipophilic
58
59
60
61
62
63
64
65

1
2
3
4 compartments of the stacked bilayers, while hydrophilic small drugs can be hosted in the
5
6 alternating hydrophilic layers, together with hydrated headgroups of the surfactant.
7
8

9
10 Finally, given the outstanding performance of Span20 NBs, and in view of the development of an
11
12 innovative theranostic platform, it was selected for a pilot test *in vivo* in a mouse model. After
13
14 administration, a rapid sustained enhancement of echographic signal for over 60 seconds (as
15
16 ethically allowed) was monitored within the mouse carotid artery (Figure 7A) demonstrating the
17
18 Span20 NBs utility as an ultrasonic contrast agent, with notable persistence. Images were acquired
19
20 both at 30MHz and at 40MHz and demonstrated marked enhancement at both frequencies (Figure
21
22 7B, 7C). Comparable enhancement is also observed for SonoVue[®] microbubbles in the 30-40MHz
23
24 frequency range, but previous experimental and modelling studies suggest that only a discrete sub-
25
26 population of SonoVue[®] bubbles contribute to signal enhancement at these high frequencies (3),
27
28 likely requiring decantation of SonoVue[®] for signal optimization. Conversely, as shown in the
29
30 preceding sections, Span20 NBs are smaller in size, and relatively mono-disperse, and their
31
32 resonance frequency is much higher (> 20 MHz, Figure S1). The present *in vivo* pilot test, then,
33
34 highlights the potential of Span20 NBs as a contrast agent for preclinical imaging studies and for
35
36 small animal veterinary applications.
37
38
39
40
41
42
43
44
45
46
47
48
49
50
51
52
53
54
55
56
57
58
59
60
61
62
63
64
65

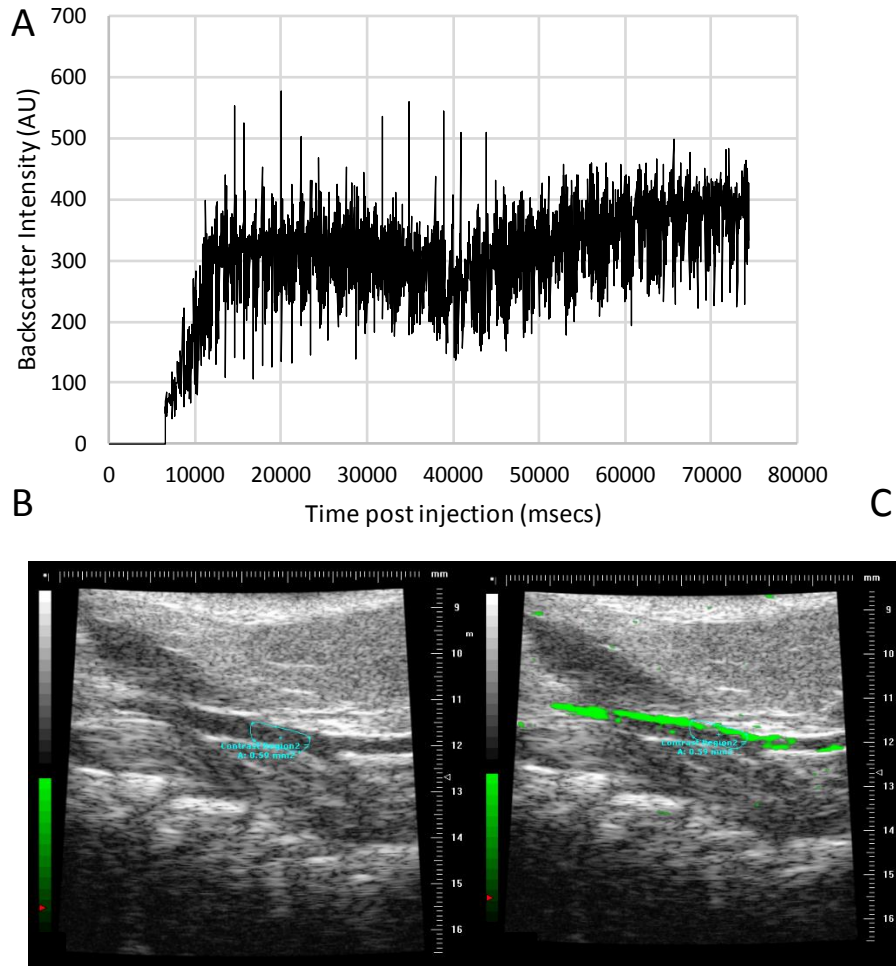


Figure 7. A) Backscatter enhancement relative to mean reference baseline measurements, measured in carotid artery before, during and after a contrast injection of 50 microlitres of Span-20 nanobubbles. B) Baseline image of mouse carotid artery showing region-of-interest, outlined in blue. C) Contrast-enhanced image with green showing presence of contrast. Images acquired at 30MHz using a Vevo 770 preclinical ultrasound scanner.

1
2
3
4 **Conclusions**
5
6

7
8 The proposed NBs formulation, prepared according to the described protocol, demonstrates
9
10 physical and chemical properties suitable for it to be applied as multipurpose agent for US-assisted
11
12 applications. Detailed characterization and focused tests show that NBs display key structural
13
14 features, namely, they are constituted by a monodisperse and ultra-stable population of shelled
15
16 nano-sized bubbles, stabilized by an amphiphilic multilamellar envelope. The NBs efficiently
17
18 entrap the non-toxic PFC gas at physiological temperature and perform as good acoustic enhancers
19
20 over a wide frequency range and out of resonant conditions, as tested in both *in vitro* and *in vivo*
21
22 experiments. The structural stability of NBs ensures a durable acoustic efficiency, as the presence
23
24 of the closed amphiphilic shell appears to constitute a good structural barrier against collapse or
25
26 gas diffusion and leakage, thus improving the persistence of US contrast in diagnostics. The time
27
28 stability of their formulation in the form of aqueous dispersions distinguishes these NBs as
29
30 compared to current marketed products, that are lyophilized and dehydrated to be stored, and then
31
32 need to be reconstituted before use. Of note, the possibility to co-load hydrophilic and lipophilic
33
34 therapeutic and/or diagnostic agents in the amphiphilic envelope of NBs, without depleting their
35
36 US performance, illustrates their potential as a platform for the design and production of versatile
37
38 carriers to be used in US-assisted diagnostic, therapeutic and theranostic applications.
39
40
41
42
43
44
45
46
47
48
49

50
51 **Abbreviations**
52

53 FDA, Food and Drug Administration; US, ultrasound; MBs, microbubbles; NBs, nanobubbles.
54
55
56
57
58

59 **Competing Interests**
60
61
62
63
64
65

1
2
3
4 The authors declare the following competing financial interest(s): The authors Federica Rinaldi,
5
6 Carlotta Marianecchi, Maria Carafa and Andrea Bettucci are inventors of a patent on the
7
8 nanobubbles used in the present research. The other co-authors have no conflict of interest.
9
10

11 **Acknowledgment**

12
13
14
15 We thank ESRF and ID02 staff for beamtime and assistance (10.15151/ESRF-ES-281427365).
16
17 E.D.F. thanks BIOMETRA Dept. for partial support (PSR2020_DEL_FAVERO).
18
19
20
21
22
23

24 **References**

- 25
26
27 1. Feinstein SB, Shah PM, Bing RJ, Meerbaum S, Corday E, Chang B-L, et al. Microbubble
28 dynamics visualized in the intact capillary circulation. *Journal of the American College of*
29 *Cardiology*. 1984;4(3):595-600.
- 30
31 2. Frinking P, Segers T, Luan Y, Tranquart F. Three decades of ultrasound contrast agents: a
32 review of the past, present and future improvements. *Ultrasound in medicine & biology*.
33 2020;46(4):892-908.
- 34
35 3. Sun C, Sboros V, Butler MB, Moran CM. In vitro acoustic characterization of three
36 phospholipid ultrasound contrast agents from 12 to 43 MHz. *Ultrasound in medicine & biology*.
37 2014;40(3):541-50.
- 38
39 4. Lee JY, Minami Y, Choi BI, Lee WJ, Chou Y-H, Jeong WK, et al. The AFSUMB
40 consensus statements and recommendations for the clinical practice of contrast-enhanced
41 ultrasound using sonazoid. *Journal of Medical Ultrasound*. 2020;28(2):59.
- 42
43 5. Dietrich CF, Nolsøe CP, Barr RG, Berzigotti A, Burns PN, Cantisani V, et al. Guidelines
44 and good clinical practice recommendations for contrast enhanced ultrasound (CEUS) in the liver–
45 update 2020–WFUMB in cooperation with EFSUMB, AFSUMB, AIUM, and FLAUS. *Ultraschall*
46 *in der Medizin-European Journal of Ultrasound*. 2020;41(05):562-85.
- 47
48 6. Zlitni A, Gambhir SS. Molecular imaging agents for ultrasound. *Current opinion in*
49 *chemical biology*. 2018;45:113-20.
- 50
51 7. Kooiman K, Roovers S, Langeveld SA, Kleven RT, Dewitte H, O'Reilly MA, et al.
52 Ultrasound-responsive cavitation nuclei for therapy and drug delivery. *Ultrasound in Medicine &*
53 *Biology*. 2020;46(6):1296-325.
- 54
55 8. Ingram N, McVeigh LE, Abou-Saleh RH, Maynard J, Peyman SA, McLaughlan JR, et al.
56 Ultrasound-triggered therapeutic microbubbles enhance the efficacy of cytotoxic drugs by
57 increasing circulation and tumor drug accumulation and limiting bioavailability and toxicity in
58 normal tissues. *Theranostics*. 2020;10(24):10973.
- 59
60 9. Logan K, Foglietta F, Nesbitt H, Sheng Y, McKaig T, Kamila S, et al. Targeted chemo-
61 sonodynamic therapy treatment of breast tumours using ultrasound responsive microbubbles
62
63
64
65

- 1
2
3
4 loaded with paclitaxel, doxorubicin and Rose Bengal. *European journal of pharmaceutics and*
5 *biopharmaceutics.* 2019;139:224-31.
- 6
7 10. Nesbitt H, Sheng Y, Kamila S, Logan K, Thomas K, Callan B, et al. Gemcitabine loaded
8 microbubbles for targeted chemo-sonodynamic therapy of pancreatic cancer. *Journal of controlled*
9 *release.* 2018;279:8-16.
- 10
11 11. Wu H, Abenojar EC, Perera R, An T, Exner AA. Time-intensity-curve analysis and tumor
12 extravasation of nanobubble ultrasound contrast agents. *Ultrasound in medicine & biology.*
13 2019;45(9):2502-14.
- 14
15 12. Fang J, Nakamura H, Maeda H. The EPR effect: unique features of tumor blood vessels
16 for drug delivery, factors involved, and limitations and augmentation of the effect. *Advanced drug*
17 *delivery reviews.* 2011;63(3):136-51.
- 18
19 13. Jadhav AJ, Barigou M. Bulk nanobubbles or not nanobubbles: that is the question.
20 *Langmuir.* 2020;36(7):1699-708.
- 21
22 14. Omata D, Maruyama T, Unga J, Hagiwara F, Munakata L, Kageyama S, et al. Effects of
23 encapsulated gas on stability of lipid-based microbubbles and ultrasound-triggered drug delivery.
24 *Journal of Controlled Release.* 2019;311:65-73.
- 25
26 15. Lin C-Y, Pitt WG. Acoustic droplet vaporization in biology and medicine. *BioMed*
27 *research international.* 2013;2013.
- 28
29 16. Li DS, Schneewind S, Bruce M, Khaing Z, O'Donnell M, Pozzo L. Spontaneous nucleation
30 of stable perfluorocarbon emulsions for ultrasound contrast agents. *Nano letters.* 2018;19(1):173-
31 81.
- 32
33 17. Batchelor DV, Armistead FJ, Ingram N, Peyman SA, McLaughlan JR, Coletta PL, et al.
34 Nanobubbles for therapeutic delivery: production, stability and current prospects. *Current Opinion*
35 *in Colloid & Interface Science.* 2021;54:101456.
- 36
37 18. Perera R, Hernandez C, Cooley M, Jung O, Jeganathan S, Abenojar E, et al. Contrast
38 enhanced ultrasound imaging by nature-inspired ultrastable echogenic nanobubbles. *Nanoscale.*
39 2019;11(33):15647-58.
- 40
41 19. Eklund F, Alheshibri M, Swenson J. Differentiating bulk nanobubbles from nanodroplets
42 and nanoparticles. *Current Opinion in Colloid & Interface Science.* 2021;53:101427.
- 43
44 20. Beltramo PJ, Gupta M, Alicke A, Liascukiene I, Gunes DZ, Baroud CN, et al. Arresting
45 dissolution by interfacial rheology design. *Proceedings of the National Academy of Sciences.*
46 2017;114(39):10373-8.
- 47
48 21. Taccoen N, Lequeux F, Gunes DZ, Baroud CN. Probing the mechanical strength of an
49 armored bubble and its implication to particle-stabilized foams. *Physical Review X.*
50 2016;6(1):011010.
- 51
52 22. Batchelor DV, Abou-Saleh RH, Coletta PL, McLaughlan JR, Peyman SA, Evans SD.
53 Nested nanobubbles for ultrasound-triggered drug release. *ACS applied materials & interfaces.*
54 2020;12(26):29085-93.
- 55
56 23. Hernandez C, Nieves L, de Leon AC, Advincula R, Exner AA. Role of surface tension in
57 gas nanobubble stability under ultrasound. *ACS applied materials & interfaces.* 2018;10(12):9949-
58 56.
- 59
60 24. Schutt EG, Klein DH, Mattrey RM, Riess JG. Injectable microbubbles as contrast agents
61 for diagnostic ultrasound imaging: the key role of perfluorochemicals. *Angewandte Chemie*
62 *International Edition.* 2003;42(28):3218-35.
- 63
64 25. Kremer JR, Mastrorade DN, McIntosh JR. Computer visualization of three-dimensional
65 image data using IMOD. *Journal of structural biology.* 1996;116(1):71-6.

- 1
- 2
- 3
- 4 26. Doucet M, Cho J, Alina G, Bakker J, Bouwman W, Butler P, et al. SasView version 4.2.
- 5 2. 2019.
- 6
- 7 27. Lentz BR. Membrane “fluidity” as detected by diphenylhexatriene probes. *Chemistry and*
- 8 *Physics of Lipids*. 1989;50(3-4):171-90.
- 9
- 10 28. Alippi A, Bettucci A, Biagioni A, D’Orazio A, Germano M, Passeri D. Photoacoustic cell
- 11 for ultrasound contrast agent characterization. *Review of scientific instruments*.
- 12 2010;81(10):104903.
- 13
- 14 29. Xu J, Salari A, Wang Y, He X, Kerr L, Darbandi A, et al. Microfluidic Generation of
- 15 Monodisperse Nanobubbles by Selective Gas Dissolution. *Small*. 2021;17(20):2100345.
- 16
- 17 30. Zhang J, Chen Y, Deng C, Zhang L, Sun Z, Wang J, et al. The optimized fabrication of a
- 18 novel nanobubble for tumor imaging. *Frontiers in pharmacology*. 2019;10:610.
- 19
- 20 31. Van der Meer S, Versluis M, Lohse D, Chin C, Bouakaz A, De Jong N, editors. The
- 21 resonance frequency of sonovue/spl trade/as observed by high-speed optical imaging. *IEEE*
- 22 *Ultrasonics Symposium*, 2004; 2004: IEEE.
- 23
- 24 32. Zemb T, Lindner P. Neutron, X-rays and light. Scattering methods applied to soft
- 25 condensed matter: North Holland; 2002.
- 26
- 27 33. Rinaldi F, del Favero E, Moeller J, Hanieh PN, Passeri D, Rossi M, et al. Hydrophilic silver
- 28 nanoparticles loaded into niosomes: Physical–chemical characterization in view of biological
- 29 applications. *Nanomaterials*. 2019;9(8):1177.
- 30
- 31 34. Marianecci C, Di Marzio L, Del Favero E, Cantù L, Brocca P, Rondelli V, et al. Niosomes
- 32 as drug nanovectors: multiscale pH-dependent structural response. *Langmuir*. 2016;32(5):1241-9.
- 33
- 34
- 35
- 36
- 37
- 38
- 39
- 40
- 41
- 42
- 43
- 44
- 45
- 46
- 47
- 48
- 49
- 50
- 51
- 52
- 53
- 54
- 55
- 56
- 57
- 58
- 59
- 60
- 61
- 62
- 63
- 64
- 65



Click here to access/download
Supplementary Material
supplementary material 1905.pdf



HIGHLIGHTS

- Generation of stable gas-filled nanobubbles
- Nanobubbles are long-lived thanks to their multi-layered lipid/surfactant shell
- Nanobubbles can carry lipophilic and hydrophilic drugs
- Nanobubbles perform as good acoustic enhancers *in vitro*
- Nanobubbles are useful contrast agents in *in vivo pilot test* in a mouse model

CRediT author statement

Patrizia N Hanieh, Caterina Ricci, Federica Rinaldi, Elena Del Favero, Carlotta Marianecchi: Conceptualization, Investigation, Writing- Original draft preparation, **Andrea Bettucci, Laura Cantù:** Investigation, Data curation, Writing- Original draft preparation. **Roberto Marotta:** Investigation. **Carmel M Moran:** Data curation, Supervision. **Maria Carafa:** Conceptualization. **All authors:** Writing- Reviewing and Editing,